Biochimica et Biophysica Acta 1818 (2012) 2135–2148

Contents lists available at SciVerse ScienceDirect

Biochimica et Biophysica Acta

journal homepage: www.elsevier.com/locate/bbamem

Molecular structures of fluid phase phosphatidylglycerol bilayers as determined by small angle neutron and X-ray scattering

Jianjun Pan [a,*], Frederick A. Heberle [a], Stephanie Tristram-Nagle [b], Michelle Szymanski [c], Mary Koepfinger [c], John Katsaras [a,d,e], Norbert Kučerka [e,f]

[a] Biology and Soft Matter Division, Neutron Sciences Directorate, Oak Ridge National Laboratory, Oak Ridge, TN 37831-6100, USA
[b] Biological Physics Group, Department of Physics, Carnegie Mellon University, Pittsburgh, PA 15213, USA
[c] Douglass Residential College, Rutgers University, New Brunswick, NJ 08901, USA
[d] Joint Institute for Neutron Sciences, Oak Ridge National Laboratory, Oak Ridge, TN 37831-6453, USA
[e] Canadian Neutron Beam Centre, National Research Council, Chalk River, Ontario, Canada K0J 1J0
[f] Department of Physical Chemistry of Drugs, Faculty of Pharmacy, Comenius University, Odbojárov 10, 832 32 Bratislava, Slovakia

ARTICLE INFO

Article history:
Received 19 December 2011
Received in revised form 22 March 2012
Accepted 7 May 2012
Available online 11 May 2012

Keywords:
Lipid bilayer
Bilayer structure
Area per lipid
Bilayer thickness
Molecular dynamics simulations
Fluid phase

ABSTRACT

We have determined the molecular structures of commonly used phosphatidylglycerols (PGs) in the commonly accepted biologically relevant fluid phase. This was done by simultaneously analyzing small angle neutron and X-ray scattering data, with the constraint of measured lipid volumes. We report the temperature dependence of bilayer parameters obtained using the one-dimensional scattering density profile model – which was derived from molecular dynamics simulations – including the area per lipid, the overall bilayer thickness, as well as other intrabilayer parameters (e.g., hydrocarbon thickness). Lipid areas are found to be larger than their phosphatidylcholine (PC) counterparts, a result likely due to repulsive electrostatic interactions taking place between the charged PG headgroups even in the presence of sodium counterions. In general, PG and PC bilayers show a similar response to changes in temperature and chain length, but differ in their response to chain unsaturation. For example, compared to PC bilayers, the inclusion of a first double bond in PG lipids results in a smaller incremental change to the area per lipid and bilayer thickness. However, the extrapolated lipid area of saturated PG lipids to infinite chain length is found to be similar to that of PCs, an indication of the glycerol–carbonyl backbone's pivotal role in influencing the lipid–water interface.

Published by Elsevier B.V.

1. Introduction

Cells have evolved to manufacture a remarkable number of lipid species, which differ in the degree of hydrocarbon chain unsaturation and in the chemical nature of their polar headgroups. Phospholipids alone count five major headgroup modifications to their phosphatidic acid precursor. Under neutral pH conditions, these include electrically neutral (i.e., choline or ethanolamine) and negatively charged (i.e., serine, inositol, or glycerol) headgroups. Therefore, a major challenge in membrane biology is to understand the functional significance of this headgroup diversity [1]. For example, a given mixture of neutral and anionic lipids in a membrane confers a surface charge density that not only influences the membrane's permeability to ions and charged molecules, but can also affect the function of membrane proteins. Among the charged headgroup moieties, glycerol possesses unique structural properties that mimic water, conferring an increased solvation and hydrogen bonding capacity [2]. Phosphatidylglycerols (PGs) may therefore have specialized structural and functional properties in membranes, beyond those that can be attributed to their inherent net negative charge.

The PG content found in biological membranes varies widely between organisms, and even among the various membranes within a given organism. While relatively rare in mammalian membranes, PG is omnipresent in the thylakoid membranes of higher plants and cyanobacteria, where it contributes to the assembly and stability of photosystem I and II protein complexes [3]. PG is also the predominant anionic bacterial lipid. The inner bacterial membrane is composed primarily of phosphatidylethanolamine (PE) and PG, with PG typically constituting 20–25 mol% of the total lipid content, although up to 60 mol% is found in some species. The particular role of PG in bacterial defense mechanisms has also received considerable attention. Bacteria are known to adjust their PE/PG ratio upon exposure to toxic organic solvents, a scenario which presumably alters their surface charge density and lipid area (minimizing permeability to the toxin), while preserving bilayer integrity [4]. It is also clear that surface charge density is critical to the function of antimicrobial peptides (AMPs), which despite their wide diversity in structure and mechanisms of

* Corresponding author at: One Bethel Valley Road, Oak Ridge National Laboratory, Neutron Scattering Science Division, Building 8630, Room B110, Oak Ridge, TN 37830-6100, USA. Tel.: +1 865 576 5841.
E-mail address: panj@ornl.gov (J. Pan).

0005-2736/$ – see front matter. Published by Elsevier B.V.
doi:10.1016/j.bbamem.2012.05.007

action, share a net cationic feature [5]. For example, some bacteria are able to decrease their vulnerability to cationic polypeptides by neutralizing PG through the addition of lysine, while mutants lacking this ability show higher susceptibility to a number of different AMPs [6–8].

Through the ever-increasing availability of high-performance computational resources, molecular dynamics (MD) simulations have emerged as powerful and indispensable tools for elucidating the structure and dynamics of biomembrane systems, down to the level of individual atoms. For example, MD simulations have been utilized to gain insight into lipid–lipid and lipid–protein interactions in bacterial membrane models. Simulations of model membranes consisting of PE and PG suggest that PG increases the number of hydrogen bonds created by PE, a mechanism which may help stabilize bacterial membranes and reduce their permeability to small organic solvent molecules [9,10]. Substantially increased PE hydrogen bonding in the presence of PG has also been observed in simulations by Zhao et al., who noted reduced PE headgroup mobility and protrusion at the aqueous interface. They similarly concluded a reduction in membrane permeability and increased membrane stabilization [11]. The interaction of AMPs with POPG bilayers has been examined using atomistic [12] and coarse-grained [13] MD simulations, with both studies finding a strong, favorable entropic contribution to the binding free energy — an observation associated with the release of counterions from the membrane interface. Simulations have also suggested a potential role for PG-rich membrane domains in the action of AMPs [14].

MD studies of single-component bilayers are particularly important for assessing the ability of simulation conditions (e.g., force fields, protonation state, and other physical parameters) to reproduce experimental data. One surprising MD result was the observation of a much smaller POPG lipid area, as compared to POPC under the same conditions. Despite their similar transition temperatures, POPG was found to have an area of 55 $Å^2$ at 37 °C, compared to 65 $Å^2$ for POPC [15]. The nearly 20% reduction in area per lipid is, however, counterintuitive given the likelihood of repulsive electrostatic interactions taking place among the PG headgroups. A subsequent MD study reproduced this result, finding that PG electrostatic repulsion was attenuated by increased intra- and inter-molecular hydrogen bonding and strong ion–lipid interactions [11]. Zhao et al. concluded that the presence of large ion–lipid clusters with highly polar interfacial interactions provides a potential molecular mechanism for the low permeability of bacterial membranes to organic solvents. Other simulations using the GROMACS force field and conditions of zero surface tension have since reproduced the smaller area per lipid, increased hydrocarbon chain order and reduced fluidity of POPG bilayers — as compared to those made of POPC [16–18].

In addition to GROMACS simulations, a handful of POPG studies have been performed using the CHARMM27 force field. In contrast to the above-mentioned studies, Tolokh et al. and Henin et al. reported lipid areas of 66.4 and 65.0 $Å^2$, respectively, for POPG at 37 °C under conditions of zero surface tension [12,19]. While still finding substantial hydrogen bonding and ion–lipid interactions, Tolokh et al. concluded that the details of these interactions (particularly of the specific atoms involved) are significantly different from those reported in the previous POPG simulations. Broemstrup et al. looked at DMPG bilayers [20] and found that the zero surface tension condition did not accurately reproduce reported experimental values for lipid area [21] and hydrocarbon chain order [22], though good agreement could be obtained by imposing a small positive surface tension. The discrepancies between the GROMACS and CHARMM results for PG lipids highlight the strong sensitivity of MD simulations to the particular details of force fields, ensembles and the treatment of electrostatics. The well-established method of evaluating such deficiencies is through the comparison of simulated and experimentally determined information [23]. Simulations should therefore be guided by experimental data [24], thus increasing their validity when they are able to reproduce experimentally observable structural parameters [25]. Among these parameters is the average area per lipid, which has typically served as the primary validation for bilayer simulations owing to its direct relationship with other bilayer structural and dynamical properties [26]. Anezo et al. have noted that regardless of the particular force field or simulation methodology used, simulations which are able to correctly reproduce lipid areas give rise to realistic bilayer properties [26]. The lack of such experimental data for PG bilayers has proven to be an impediment to the improvement of force fields and simulation methodologies for this class of lipids.

Accurately determining the area per lipid in biologically relevant fluid bilayers is not straightforward, and significant discrepancies exist in the literature [27]. We have recently developed a hybrid experimental/computational technique (the scattering density profile, or SDP model) that addresses some of the difficulties associated with determining lipid areas [28]. The technique exploits the fact that neutron and X-ray scattering are sensitive to different bilayer thicknesses — the large difference in the neutron scattering length density (NSLD) of the proteated lipid and the deuterated water defines the overall bilayer thickness, while X-ray scattering resolves the headgroup–headgroup distance due to the large electron density (ED) contrast between the electron-rich phosphate groups and the hydrocarbon/aqueous medium. Bilayer thicknesses are in turn related to the average lipid area through molecular volumes, which are obtained through independent measurements. A key step in the SDP analysis is the use of MD simulations to "parse" the lipid molecule into components whose volume probability distributions follow simple analytical functional forms. Given the appropriate atomic scattering densities, these volume probabilities simultaneously provide a base for both the NSLD and ED profiles, and hence the scattering form factors. The bilayer structure is thus determined by varying the set of parameters describing the volume probability distributions of the molecular components in order to achieve a global best-fit to the experimentally determined neutron and X-ray scattering form factors.

We have recently published the molecular parameterization of POPG for use in the SDP model [29]. Here, we extend our analysis to the commonly used saturated, mixed chain and di-monounsaturated PG lipids, including their temperature and acyl chain length dependence of area per lipid, volume and bilayer thickness in the fluid phase.

2. Materials and methods

Synthetic saturated acyl chain phosphatidylglycerols: 1,2-dilauroyl-*sn*-glycero-3-phosphatidylglycerol (diC12:0PG, DLPG), 1,2-dimyristoyl-*sn*-glycero-3-phosphatidylglycerol (diC14:0PG, DMPG), 1,2-dipalmitoyl-*sn*-glycero-3-phosphatidylglycerol (diC16:0PG, DPPG), 1,2-distearoyl-*sn*-glycero-3-phosphatidylglycerol (diC18:0PG, DSPG), mixed acyl chain phosphatidylglycerols: 1-palmitoyl-2-oleoyl-*sn*-glycero-3-phosphatidylglycerol (C16:0–18:1PG, POPG) and 1-stearoyl-2-oleoyl-*sn*-glycero-3-phosphatidylglycerol (C18:0–18:1PG, SOPG), and the unsaturated acyl chain phosphatidylglycerol: 1,2-dioleoyl-*sn*-glycero-3-phosphatidylglycerol (diC18:1PG, DOPG) were purchased from Avanti Polar Lipids (Alabaster, AL) and used without further purification.

Samples for small angle scattering experiments were prepared by mixing ~60 mg of lipid with 1.5 ml D_2O (99.9% pure, Chalk River Laboratories), or 18 MΩcm H_2O (Millipore) solution with 100 mM NaCl, followed by temperature cycling through the lipid's main phase transition until a uniform lipid dispersion was obtained. Unilamellar vesicles (ULVs) were prepared from lipid dispersions at a temperature above each lipid's main phase transition using an Avanti mini-extruder fitted with two 0.25 ml air-tight syringes. Lipid dispersions were extruded through two polycarbonate filters (~33 total passes) with 500 Å pore diameters, resulting in ~600 Å diameter ULVs [30]. Finally, samples were diluted with D_2O or H_2O to the desired external contrast condition (i.e., 100%, 70%, and 50% D_2O in the case of neutron contrast variation

experiments and 100% H_2O in the case of X-ray scattering experiments). The total lipid concentration for all ULV samples was ~20 mg/ml, which guarantees sufficient water between ULVs to eliminate the possibility of inter-particle interactions [30].

Samples for volume measurements were prepared by weighing between 50 and 65 mg of lyophilized lipid into a 6 ml Nalgene vial. Lipid dispersions were obtained by hydrating the lipid powder with between 1.2 and 1.4 g of 100 mM NaCl solution, followed by temperature cycling (three times) between −20 and 60 °C, and vortexing at each temperature. After the first volume measurement, samples were diluted 1:1 by weight with 100 mM NaCl, and measured again to obtain an estimate of the error.

2.1. Volume determination

Lipid volumes were determined as a function of temperature (20 to 60 ± 0.01 °C) using an Anton-Paar DMA4500 (Ashland, VA) vibrating tube density meter. V_L was calculated from

$$V_L = \frac{M_L}{0.6022\rho_S}\left[1+\frac{m_W}{m_S}\left(1-\frac{\rho_S}{\rho_W}\right)\right], \quad (1)$$

where M_L is the molar mass of the lipid, ρ_S and ρ_W are the measured densities of the sample and 100 mM NaCl solution, respectively, m_W is the mass of the 100 mM NaCl solution, and m_s is the mass of the lipid in sample. Several samples were also measured using the neutral buoyancy method [31,32], which was judged to be more accurate than the vibrating tube densimetry method for 60 °C samples, due to bubble formation. However, the neutral buoyancy method was only successful for PGs with saturated chains, since those containing a monounsaturated chain did not sink over the accessible range of solvent densities in D_2O/H_2O mixtures. Based on our neutral buoyancy results, PG vesicles prepared by aqueous dispersion likely contain many lamellae in the case of saturated lipids (which separated from bulk D_2O/H_2O solutions), and perhaps only one or a few lamellae in the case of unsaturated lipids (which were not sufficiently different in density from bulk solution to settle out of solution). In contrast, the scattering data obtained in this study utilizes ULVs prepared by extrusion. Despite these differences in vesicle lamellarity, we are able to combine the volume and scattering data in a global analysis, since the volume per lipid is a well-defined physical parameter that is not affected by the number of lamellae in a vesicle (provided the vesicle is fully hydrated, as is the case in our experiments). We also note that earlier publications have established that the X-ray scattering form factor is consistent between ULVs, multilayer vesicles, and oriented multibilayer samples [33,34].

Fig. 1 shows the measured molecular lipid volumes V_L with previously published DOPC data [35] (shown for comparison). Compared to the PC lipid, a smaller volume is observed for the equivalent PG lipid, due to its smaller headgroup. The PG headgroup volume was estimated by subtracting the volume difference between a PC [31,36] and PG lipid from the PC headgroup volume of 331 Å^3 [37], assuming an invariant hydrocarbon volume between the two lipid species [i.e. $V_{HL}(PG) = V_{HL}(PC) - (V_L(PC) - V_L(PG))$, where the subscripts HL and L refer to headgroup and total lipid, respectively]. Using this method, the average PG headgroup volume was determined to be 291 ± 4 Å^3, a value which is in good agreement with the 289 Å^3 value obtained from our previous MD simulations of POPG [29]. To quantify the effect of temperature on lipid volume, we also calculated thermal volume expansivities, $\alpha^T_V = (\partial V/\partial T)_\Pi/V$ (where Π refers to constant pressure), over a range of temperatures for fluid phase PG lipids (Table 1).

2.2. Small angle X-ray scattering

X-ray data were taken at the Cornell High Energy Synchrotron Source (CHESS) G-1 station. A 1.18 Å wavelength (λ) incident X-ray beam of dimensions 0.24 × 0.24 mm^2 was detected using a 1024 × 1024 pixel array

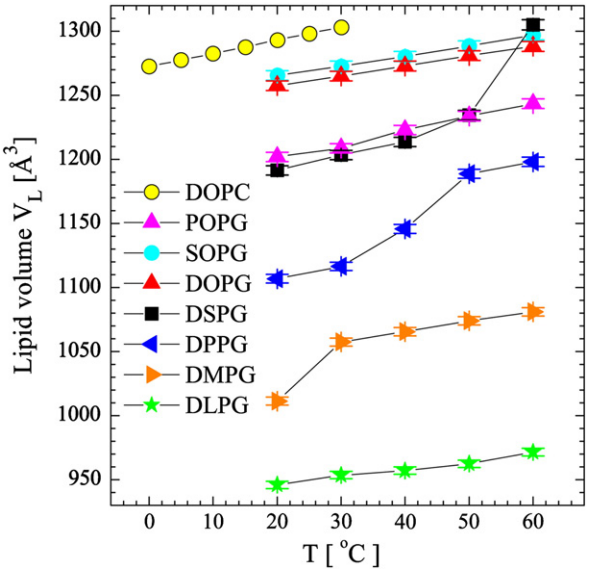

Fig. 1. PG lipid volumes obtained by vibrating tube densitometry and neutral buoyancy as described in the Materials and methods. DOPC data are shown for comparison. Uncertainties of 0.3% in the measured volumes are estimated based on the average of two samples with different lipid concentrations. For DMPG, DPPG, and DSPG bilayers, a volume jump occurs in the vicinity of the main gel-to-liquid crystalline transition: 23 °C for DMPG, 41 °C for DPPG, and 54 °C for DSPG. Lines are to guide the eye only, and do not indicate the true widths of the transitions, which are much narrower.

FLICAM charge-coupled device (CCD) with 71 μm linear dimension pixels. The sample-to-detector distance (SDD) was 423.6 mm, as determined using silver behenate (d-spacing of 58.367 Å). Samples were taken up in 1.5 mm quartz capillaries and placed in a temperature controlled, multiposition sample holder. 2D images were "de-zingered" using two consecutive 60 s exposures and corrected using calibration files supplied by CHESS. Data sets were normalized using the incident beam intensity as measured by an ion chamber, and background resulting from water and air scatter was subtracted according to the procedure described in [30]. The scattering intensity I versus scattering vector q [$q = 4\pi/\lambda \sin(\theta)$, where λ is the wavelength and 2θ is the scattering angle] was obtained through radial averaging of the corrected 2D data. As has been shown [38], the absorption coefficient of I by ULV solution is independent of q over the range studied. Therefore, no absorption correction was necessary. Finally, a linear intensity $I_b(q)$ accounting for the linear background was subtracted from the obtained scattering intensity $I(q)$. The X-ray scattering form factor, which is used to fit to our model (see Section 2.4), is related to the scattering intensity $I(q)$ by the following equation,

$$|F(q)| = \text{sign}(I(q))\sqrt{|I(q)| \times q^2}. \quad (2)$$

A typical X-ray form factor is shown in Fig. 2A. In addition to model-based analysis, these form factors can be compared directly to simulated data, as outlined in [39].

2.3. Small angle neutron scattering

Neutron scattering data were taken at the NG-3 and NG-7 stations [40] located at the National Institute of Standards and Technology (NIST) Center for Neutron Research (NCNR), and at the CG-3 Bio-SANS instrument [41] located at the Oak Ridge National Laboratory (ORNL). In all cases, 6 Å wavelength (~12% FWHM) neutrons were selected using a mechanical velocity selector. Multiple sample-to-detector distances (i.e., 1.3, 5, and 13.2 m at NG-3; 2, 5, and 15.3 m at NG-7; 2.5 and 15.3 m at CG-3) were used, resulting in a total scattering vector of $0.03 < q < 0.25$ Å^{-1}. We note that the smallest q value

Table 1
Temperature dependence of lipid volumes (Å^3) and volume thermal expansivities $\alpha^T_V = (\partial V/\partial T)_\Pi / V \times 10\text{^}4\ K^{-1}$ for fluid phase PG bilayers. A volume uncertainty of 0.3% was estimated based on densitometry measurements before and after sample dilution.

	20 °C		30 °C		40 °C		50 °C		60 °C	
	V	α^T_V	V	α^T_V	V	α^T_V	V	α^T_V	V	α^T_V
DLPG	945.9	6.3 ± 1.0	953.6	6.3 ± 1.0	957.1	6.3 ± 0.9	962.4	6.2 ± 0.9	971.5	6.2 ± 0.9
DMPG	1011.4	NA	1057.4	7.5 ± 1.4	1065.5	7.4 ± 1.3	1074.0	7.4 ± 1.3	1080.9	7.3 ± 1.3
DPPG	1106.8	NA	1116.5	NA	1145.7	NA	1188.8	7.8 ± 4.3	1198.1	7.8 ± 4.2
DSPG	1191.4	NA	1203.4	NA	1213.7	NA	1234.5	NA	1305.0	NA
POPG	1201.9	9.0 ± 1.0	1208.7	9.0 ± 1.0	1222.9	8.9 ± 1.0	1233.7	8.8 ± 0.9	1243.6	8.7 ± 0.9
SOPG	1265.5	6.2 ± 1.0	1272.8	6.2 ± 1.0	1280.3	6.2 ± 0.9	1288.6	6.1 ± 0.9	1297.1	6.1 ± 0.9
DOPG	1257.5	6.2 ± 1.0	1265.0	6.1 ± 1.0	1272.8	6.1 ± 1.0	1281.0	6.0 ± 0.9	1288.2	6.0 ± 0.9

varies somewhat for different instruments (see Supplementary materials). However, such variation does not affect our model analysis, since the relevant length scale for bilayer structure is of the order of 40 Å, and is therefore determined by data in the q range well extended above 0.05 Å^{-1}. Data were collected using a 2D ^{3}He position-sensitive detector with a 5 mm × 5 mm spatial resolution (0.64 m × 0.64 m for the instruments at NIST, and 1 m × 1 m at ORNL). Samples were taken up in standard quartz (banjo) cells. Finally, the 2D data images were corrected and reduced into 1D scattering curves using software supplied by NIST [42] and ORNL. As was the case for X-rays, no absorption correction was applied [38]. Fig. 2B shows typical neutron scattering form factors calculated using Eq. (2).

2.4. Bilayer model

The SDP model for PG lipids was developed by Kučerka et al. [29] and is graphically depicted in Fig. 2C–E. Briefly, the component groups are chosen on the basis that each group has the same functional form for all contrast conditions (i.e., ED and NSLD profiles, Fig. 2C and D, respectively). Three Gaussians are used to describe the lipid headgroup, i.e., one each for the carbonyl–glycerol (CG), phosphate (PG1), and terminal glycerol (PG2) moieties. The total hydrocarbon region (i.e., the sum of the CH_2, CH and CH_3 groups) is represented by an error function. The CH and CH_3 groups are each described by a single Gaussian, which are then subtracted from the error function to obtain the CH_2 distribution. The water distribution is defined by complementarity with the lipid components by requiring that all volume probabilities sum to unity at each value of z (Fig. 2E). In this way, the model captures all of the features of the different scattering density profiles (SDPs), while satisfying the spatial conservation principle [28]. Finally, the analytical X-ray and neutron form factors, which were used to fit the experimental scattering data, were obtained by Fourier transform of the ED and the various NSLDs based on the SDP model (Fig. 2A and B).

While a disordered fluid bilayer is inherently a low resolution structure, it is nevertheless possible (in principle) to fully resolve this low resolution structure, provided that enough independent data are acquired to account for the degrees of freedom in the model [43]. Though the SDP model addresses the resolution problem by combining multiple X-ray and neutron data sets, we determined that because of the limited q-range and counting statistics of our experimental scattering data (and in particular the three neutron data sets), a complete description of all PG structural features is not possible, as judged by the lack of stability in the unconstrained nonlinear least squares analysis. To enhance the stability and robustness of the fitting algorithm, the parameter space was restricted through a judicious choice of constraints guided by a combination of experimental and simulation data. Namely, the total lipid and headgroup volumes were fixed to experimentally determined values, as described in Section 2.1. The center of the terminal methyl Gaussian was fixed to $z = 0$ through symmetry considerations,

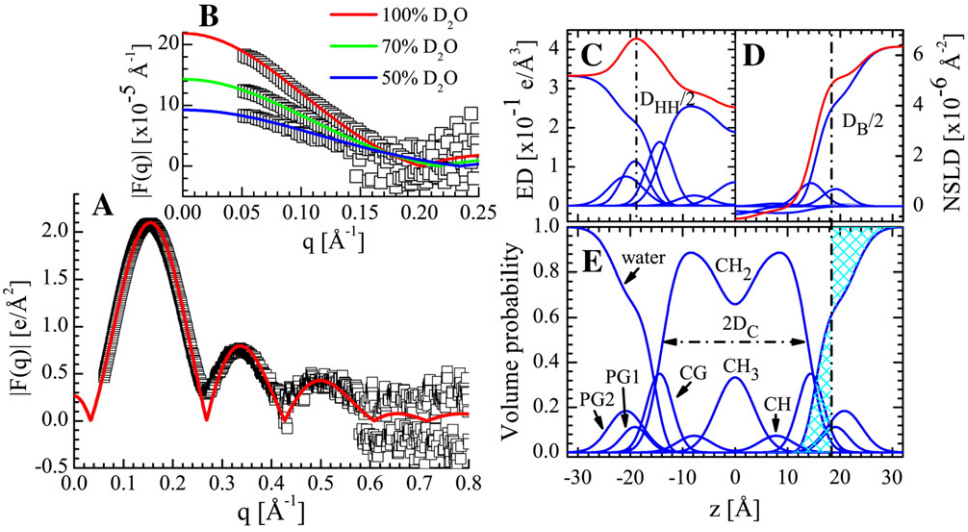

Fig. 2. SDP model fit to POPG data at 30 °C. The lipid components are described by five Gaussians and one error function. The water probability is determined by complementarity with lipid components, which ensures unity of the total volume probability (i.e., space-filling model). The component center and width are determined through simultaneous nonlinear least-squares fitting of the experimental X-ray (A) and neutron (B) form factors. The electron density (C), neutron scattering length density (D) and volume probability distributions (E) are computed based on the parameters obtained from the fits to the data. Lipid area A, overall bilayer thickness D_B, and hydrocarbon thickness $2D_C$, in addition to the other intrabilayer structural information, are determined from the profiles displayed in panels C, D, and E. The Gibbs dividing surface (shown in E) is defined as a point along the z-axis, where the integrated water distribution areas (hatched) are equal, i.e., effectively the interface between the lipid bilayer and water (i.e., $D_B/2$).

and the width of the PG2 Gaussian was set to the value obtained from MD simulations [29]. In addition to these hard constraints, several soft constraints were employed. For each soft-constrained parameter, deviation from a target value (taken to be the value obtained from MD simulations) resulted in a quadratic penalty which was added to the overall χ^2. Following [28], the penalty terms were independently scaled to allow for ~10% deviation from the target value. Soft-constrained parameters included the ratios of headgroup and acyl chain component volumes, and the width of the hydrocarbon error function.

From Fig. 2C and D it is obvious that neutrons and X-rays are sensitive to different parts of the bilayer. The ED distribution of the lipid bilayer is different from the NSLD distribution due to the different interactions of X-rays and neutrons with matter. While the scattering amplitude for X-rays increases monotonically with the increasing atomic number, the scattering amplitude for neutrons' does not follow the pattern. As a consequence, in the case of X-rays the electron dense phosphate groups contrast very well with the less electron dense hydrocarbon chain region, thus revealing the headgroup–headgroup spacing, as well as the terminal methyl groups in the bilayer center (see Fig. 2C). On the other hand, the high NSLD of D_2O amplifies the contrast between the lipid bilayer and the water phase, thus enabling the accurate determination of the total bilayer thickness (see Fig. 2D), and consequently, the area per lipid (assuming knowledge of the lipid volume). Based on the amounts and quality of the experimental data used in the analysis, we estimate an uncertainty for the various structural parameters of ~2% [28].

Although the SDP model is designed to obtain structure from neutron and X-ray scattering data, the primary description is in terms of volume probability distributions (Fig. 2E) [28]. Briefly, the component groups are chosen on the assumption that each group has the same functional form for all of the different contrast conditions, and that they all sum up to unity in volume probability space. Individual ED and NSLD profiles are then calculated from the descriptions of such functional forms in terms of volume probabilities, and then multiplied by the ED and/or NSLD of the corresponding component. For example, the volume probability of the water distribution is calculated based on a complementarity requirement that volume is conserved, and is then multiplied by its ED or NSLD to obtain its scattering density profile. In addition to satisfying the spatial conservation principle, this definition allows for a direct determination of lipid area A from the volume probability of the water distribution, $P_z(\text{water})$, which gives rise to the Gibbs dividing surface between the water and the lipid (i.e., $D_B/2$ from bilayer center, see Fig. 2). In particular, the mean position of the water distribution is defined by the equality of the integrated water probability inside the Gibbs dividing surface and the integrated deficit of water probability to the outside of this surface [28] as:

$$\int_0^{D_B/2} P_z(\text{water})dz = \int_{D_B/2}^{D/2} (1-P_z(\text{water}))dz, \quad (3)$$

where $D/2$ is a point beyond which $P_z(\text{water}) = 1$. The Gibbs dividing surface is equivalent to Luzzati's division of a two-component system consisting of water and lipid [44]. Finally, lipid area is related to the Luzzati thickness D_B by [28]

$$A = 2V_L/D_B. \quad (4)$$

From Eq. (4) it is evident that the uncertainty associated with the area per lipid is directly related to the uncertainty of our measured lipid volume and the fitted thickness, D_B.

2.5. Expansivity and contractivity

For the range of temperatures studied, bilayer structural parameters, including lipid volumes, areas, and bilayer thicknesses changed linearly. Thermal expansivity and contractivity (in units K^{-1}) were determined from the slopes (which will be referred to as expansion or contraction coefficients k, with units $Å^2\,K^{-1}$ for area and $Å\,K^{-1}$ for thickness) of the linear functions used to fit the different data, divided by the corresponding structural parameters [e.g., area thermal expansivity $\alpha_A^T = (\partial A/\partial T)_\Pi/A$, overall bilayer thickness thermal contractivity $\alpha_{DB}^T = -(\partial D_B/\partial T)_\Pi/D_B$, and hydrocarbon thickness thermal contractivity $\alpha_{2DC}^T = -(\partial 2D_C/\partial T)_\Pi/(2D_C)$, where A, D_B, and $2D_C$ are the lipid area, overall bilayer thickness and hydrocarbon thickness, respectively, and the subscript Π refers to constant pressure]. To evaluate the effect of hydrocarbon chain length nc, we defined a similar set of expansivities [e.g., area chain length expansivity $\alpha_A^{nc} = (\partial A/\partial nc)_{\Pi,T}/A$, overall bilayer thickness chain length expansivity $\alpha_{DB}^{nc} = (\partial D_B/\partial nc)_{\Pi,T}/D_B$, and hydrocarbon thickness chain length expansivity $\alpha_{2DC}^{nc} = (\partial 2D_C/\partial nc)_{\Pi,T}/(2D_C)$, where the subscripts Π and T refer to constant pressure and temperature, respectively]. Uncertainties in these quantities were estimated by Monte Carlo (MC) simulations [45]. Taking lipid area as an example, this was done as follows: a large sample of artificial data was constructed by drawing random areas from normal distributions centered at the experimentally observed areas and with standard deviations given by the estimated uncertainty of the area measurement (i.e., 2% of the observed value). The resulting in silico data sets were analyzed identically to the experimental data to generate a

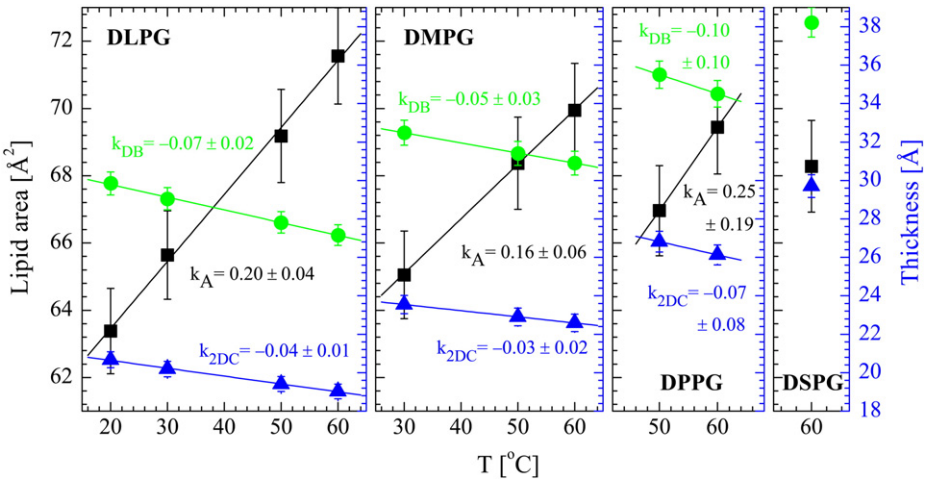

Fig. 3. Temperature dependence of DLPG, DMPG, DPPG, and DSPG lipid areas A (black squares), overall bilayer thicknesses D_B (green circles), and hydrocarbon thicknesses $2D_C$ (blue triangles). Also shown are linear least-square fits (solid lines) whose slopes are denoted by k and whose uncertainties are estimated from MC simulations.

large sample of thermal and chain-length area expansion coefficients (slopes) and expansivities (i.e., slopes divided by the corresponding areas). For a particular expansion coefficient, or expansivity, the standard deviation of its distribution is reported as the uncertainty.

3. Results

3.1. Structure of DLPG

It has been reported that both pH and cation concentration can affect the surface potential, phase transition temperature and monolayer density of DLPG [46–51]. At 100 mM ionic strength, the main gel-to-liquid crystalline transition of DLPG bilayers occurs near −5 °C [2], well below the lowest temperature we investigated (20 °C). Fig. 3 shows the temperature dependence of the main DLPG structural parameters (i.e., lipid area *A*, overall bilayer thickness D_B, and hydrocarbon chain thickness $2D_C$) obtained from the SDP model analysis utilizing one SAXS and three different contrast SANS data sets. As expected, *A* increases as a function of increasing temperature, while D_B decreases. This behavior is consistent with the greater likelihood of gauche rotamers in the acyl chains with increasing temperature – as predicted by the Boltzmann distribution – where the trans-gauche energy difference ε is about 0.5 kcal/mol/CH_2 [52].

The Boltzmann distribution also implies that as temperature continues to increase, changes in structural parameters will become smaller, and eventually vanish. However, because of the relatively narrow temperature range investigated (20 to 60 °C), the structural parameters can be approximated by a linear relation as a function of temperature (i.e., Fig. 3). Over this temperature range, DLPG's area changes by about 2.0 Å^2 for each 10 °C increase in temperature, close to the 1.7 Å^2 change observed for its neutral counterpart, DLPC [38]. Although both the overall bilayer thickness and the hydrocarbon thickness decrease as temperature increases, the changes to D_B are slightly more dramatic, suggesting a thermal thinning of the headgroup region.

As stated in the Materials and methods section, our analysis assumes a fixed headgroup volume. To evaluate the validity of such an approximation, we also analyzed the experimental data assuming the same volume thermal expansion coefficient for DLPG's headgroup and hydrocarbon chains at 60 °C, where the volume expansion is maximal. The area per lipid varies by less than 0.1%, much less than its estimated 2% uncertainty. In light of this observation, a fixed headgroup volume was used to analyze the remaining data sets.

To facilitate comparisons of structure parameters from other lipids, we calculated the area thermal expansivity α^T_A, overall bilayer thickness thermal contractivity α^T_{DB}, and hydrocarbon thickness thermal contractivity α^T_{2DC}, at each temperature (Tables 2–4). α^T_A decreases slightly as temperature increases, due to a larger area value in the denominator [i.e., $\alpha^T_A = (\partial A/\partial T)_{\Pi}/A$]. Similarly, the two thickness contractivities increase slightly with increasing temperature, due to their smaller associated thicknesses [i.e., $\alpha^T_{DB} = -(\partial D_B/\partial T)_{\Pi}/D_B$ and $\alpha^T_{2DC} = -(\partial 2D_C/\partial T)_{\Pi}/(2D_C)$]. The overall area expansivity and thickness contractivity of DLPG are very similar to DLPC bilayers [38], indicating that the hydrocarbon chain region is most affected by increasing temperature.

3.2. Structure of DMPG

Compared to DLPG, DMPG has two additional methylene groups in each of its hydrocarbon chains. It is one of the most studied anionic lipids due to its easily accessible main phase transition temperature (i.e., ~23 °C). Numerous studies have shown that DMPG exhibits a broad spectrum of phase polymorphism at low temperatures, depending on pH, ionic strength, lipid concentration, temperature, and incubation period [53–58], and references therein. Other interesting phenomena such as vesicle aggregation induced by high concentration of monovalent cations have also been reported [59].

Table 2
Lipid areas *A* (Å^2) as a function of temperature, hydrocarbon chain length, and the degree of hydrocarbon chain unsaturation. Lipid area thermal and chain length expansivities, α^T_A and α^{nc}_A, respectively, are also shown. α^{nc}_A is calculated for each group of lipids depending on their total number of double bonds (e.g., 0 for DLPG, 1 for POPG, and 2 for DOPG).

	20 °C			30 °C			50 °C			60 °C		
	A	α^T_A	α^{nc}_A	*A*	α^T_A	α^{nc}_A	*A*	α^T_A	α^{nc}_A	*A*	α^T_A	α^{nc}_A
DLPG	63.4	0.0031 ± 0.0007	NA	65.6	0.0030 ± 0.0007	−0.0042 ± 0.0140	69.2	0.0029 ± 0.0006	−0.0081 ± 0.0070	71.6	0.0028 ± 0.0006	−0.0072 ± 0.0044
DMPG	NA	NA	NA	65.1	0.0025 ± 0.0010	−0.0043 ± 0.0142	68.4	0.0024 ± 0.0009	−0.0081 ± 0.0070	69.9	0.0023 ± 0.0009	−0.0074 ± 0.0045
DPPG	NA	NA	NA	NA	NA	NA	67.0	0.0037 ± 0.0029	−0.0083 ± 0.0072	69.4	0.0036 ± 0.0028	−0.0074 ± 0.0045
DSPG	NA	NA	NA	NA	NA	NA	NA	NA	NA	68.3	NA	−0.0076 ± 0.0046
POPG	64.4	0.0027 ± 0.0007	0.0126 ± 0.0285	66.1	0.0026 ± 0.0006	0.0083 ± 0.0283	69.5	0.0025 ± 0.0006	−0.0008 ± 0.0284	71.3	0.0024 ± 0.0006	−0.0051 ± 0.0283
SOPG	65.2	0.0022 ± 0.0007	0.0125 ± 0.0281	66.7	0.0021 ± 0.0006	0.0083 ± 0.0280	69.4	0.0020 ± 0.0006	−0.0008 ± 0.0284	70.9	0.0020 ± 0.0006	−0.0052 ± 0.0284
DOPG	69.4	0.0015 ± 0.0007	NA	70.8	0.0015 ± 0.0006	NA	72.9	0.0014 ± 0.0006	NA	73.6	0.0014 ± 0.0006	NA

Table 3
Overall bilayer thicknesses D_B (Å) as a function of temperature, hydrocarbon chain length, and the degree of hydrocarbon chain unsaturation. Overall bilayer thickness thermal contractivities and chain length expansivities, α^{T}_{DB} and α^{nc}_{DB}, respectively, are also shown. α^{nc}_{DB} is calculated for each group of lipids depending on their total number of double bonds (e.g., 0 for DLPG, 1 for POPG, and 2 for DOPG).

	20 °C			30 °C			50 °C			60 °C		
	D_B	α^{T}_{DB}	α^{nc}_{DB}	D_B	α^{T}_{DB}	α^{nc}_{DB}	D_B	α^{T}_{DB}	α^{nc}_{DB}	D_B	α^{T}_{DB}	α^{nc}_{DB}
DLPG	29.9	0.0022 ± 0.0006	NA	29.1	0.0023 ± 0.0006	0.0592 ± 0.0150	27.8	0.0024 ± 0.0006	0.0691 ± 0.0081	27.2	0.0024 ± 0.0007	0.0678 ± 0.0055
DMPG	NA	NA	NA	32.5	0.0016 ± 0.0009	0.0529 ± 0.0134	31.4	0.0017 ± 0.0009	0.0612 ± 0.0072	30.9	0.0017 ± 0.0009	0.0595 ± 0.0048
DPPG	NA	NA	NA	NA	NA	NA	35.5	0.0028 ± 0.0028	0.0541 ± 0.0064	34.5	0.0029 ± 0.0029	0.0533 ± 0.0043
DSPG	NA	NA	NA	NA	NA	NA	NA	NA	NA	38.2	NA	0.0481 ± 0.0039
POPG	37.3	0.0016 ± 0.0006	0.0500 ± 0.0289	36.6	0.0016 ± 0.0006	0.0442 ± 0.0289	35.5	0.0017 ± 0.0006	0.0449 ± 0.0288	34.9	0.0017 ± 0.0007	0.0484 ± 0.0289
SOPG	38.8	0.0014 ± 0.0006	0.0385 ± 0.0278	38.2	0.0015 ± 0.0006	0.0423 ± 0.0277	37.1	0.0015 ± 0.0006	0.0430 ± 0.0276	36.6	0.0015 ± 0.0007	0.0461 ± 0.0276
DOPG	36.3	0.0007 ± 0.0006	NA	35.7	0.0008 ± 0.0006	NA	35.1	0.0009 ± 0.0006	NA	35.0	0.0009 ± 0.0006	NA

Table 4
Hydrocarbon thicknesses $2D_C$ (Å) as a function of temperature, hydrocarbon chain length, and the degree of hydrocarbon chain unsaturation. Hydrocarbon thickness expansivities as a function of temperature and hydrocarbon chain length, α^{T}_{2DC} and α^{nc}_{2DC}, respectively, are also shown. α^{nc}_{2DC} is calculated for each group of lipids depending on their total number of double bonds (e.g., 0 for DLPG, 1 for POPG, and 2 for DOPG).

	20 °C			30 °C			50 °C			60 °C		
	$2D_C$	α^{T}_{2DC}	α^{nc}_{2DC}	$2D_C$	α^{T}_{2DC}	α^{nc}_{2DC}	$2D_C$	α^{T}_{2DC}	α^{nc}_{2DC}	$2D_C$	α^{T}_{2DC}	α^{nc}_{2DC}
DLPG	20.7	0.0020 ± 0.0006	NA	20.2	0.0020 ± 0.0006	0.0832 ± 0.0153	19.4	0.0020 ± 0.0006	0.0955 ± 0.0085	19.0	0.0020 ± 0.0007	0.0936 ± 0.0059
DMPG	NA	NA	NA	23.6	0.0014 ± 0.0009	0.0714 ± 0.0131	22.9	0.0014 ± 0.0009	0.0809 ± 0.0072	22.6	0.0014 ± 0.0009	0.0788 ± 0.0049
DPPG	NA	NA	NA	NA	NA	NA	26.8	0.0026 ± 0.0028	0.0691 ± 0.0062	26.1	0.0027 ± 0.0029	0.0681 ± 0.0043
DSPG	NA	NA	NA	NA	NA	NA	NA	NA	NA	29.7	NA	0.0599 ± 0.0037
POPG	28.3	0.0012 ± 0.0006	0.0566 ± 0.0290	27.8	0.0012 ± 0.0006	0.0609 ± 0.0292	27.1	0.0012 ± 0.0006	0.0589 ± 0.0291	26.7	0.0012 ± 0.0007	0.0618 ± 0.0291
SOPG	29.9	0.0013 ± 0.0006	0.0535 ± 0.0275	29.5	0.0013 ± 0.0006	0.0574 ± 0.0276	28.7	0.0013 ± 0.0006	0.0556 ± 0.0275	28.4	0.0013 ± 0.0006	0.0582 ± 0.0274
DOPG	27.9	0.0007 ± 0.0006	NA	27.5	0.0007 ± 0.0006	NA	27.2	0.0007 ± 0.0006	NA	27.1	0.0007 ± 0.0006	NA

The main transition of DMPG from the crystalline gel to the liquid-like fluid phase occurs near 23 °C [2,54,60–63], consistent with our volume and SAXS data, which show distinguishable differences between gel phase (at 20 °C, data not shown) and fluid phase (at 30 °C) form factors. The melting temperature of DMPG is very similar to that of DMPC at 24 °C [31], indicative of the important role of DMPG's hydrocarbon chains in the gel-to-liquid crystalline transition. The X-ray form factor of DMPG bilayers shown in Fig. S6 (Supplementary materials) reveals non-zero minima for the first three lobes at 30 °C, a possible sign of bilayer asymmetry [30]. Similar form factors have also been observed in PC lipids at temperatures close to the phase transition [38]. However, because our current SDP model assumes a symmetric bilayer, a larger uncertainty should be considered to the structural parameters derived from the 30 °C data.

The structural parameters and their thermal derivatives for DMPG at 30, 50, and 60 °C are shown in Fig. 3 and Tables 2–4. Similar to DLPG, lipid area increases and bilayer thickness decreases as temperature increases. Because only three data points are available, the estimated uncertainties are larger than for the corresponding DLPG parameters. Although there is a lack of experimentally determined areas for fluid phase DMPG bilayers, our extrapolated area per lipid at 27 °C (64.5 $Å^2$) is somewhat larger than the value of 62 ± 2 $Å^2$ value obtained from a Langmuir monolayer study [21]. Moreover, our interpolated DMPG lipid area at 37 °C (66.2 $Å^2$) highlights the underestimated DMPG lipid areas reported by two previous MD studies, namely 58.5 $Å^2$ [19] and 61.8 ± 1.2 $Å^2$ [20].

3.3. Structure of DPPG and DSPG

Compared to DMPG, DPPG has two additional methylene groups in each of its hydrocarbon chains. Various thermotropic, structural, and ionic properties of DPPG bilayers have been reported, including: a) the effect of pH on chain tilt, fluidity, transition temperature, ion penetration, and surface water structure [48,64,65]; b) the effect of temperature and monovalent salt concentration (by small and wide angle X-ray scattering) in the crystalline gel phase [66]; c) divalent cation induced vesicle fusion [67]; d) a low-temperature incubation induced subgel phase [68–70], not unlike DPPC bilayers [71,72]; e) monovalent cation dependent phase behavior [61,73–75]; f) tris buffer induced acyl chain interdigitation in crystalline bilayers [76]; g) phase behavior in binary mixtures with cardiolipin [77]; and h) hydrogen bond formation with PE lipids in mixed Langmuir monolayers mimicking bacterial inner membranes [78]. MD simulations have also been performed on fluid DPPG monolayers with different area densities [79], and on DPPG/drug systems of different charge [80].

Differential scanning calorimetry measurements indicate that a sharp, highly enthalpic gel-to-liquid crystalline transition takes place near 41 °C in DPPG bilayers [2,54,62], consistent with our volume and scattering data, and similar to the melting transition temperature of DPPC. The structural parameters of DPPG fluid phase bilayers (i.e., 50 and 60 °C) obtained from the SDP model analysis are shown in Fig. 3. Because only 2 data points are available, the estimated uncertainties based on MC simulations are much larger than those of DLPG and DMPG bilayers. Nevertheless, there is a clear trend indicating that a higher temperature results in a larger area per lipid and consequently a thinner bilayer.

In contrast to the three aforementioned saturated PG lipids, not much is known about DSPG — except for two reports pertaining to bilayer interactions, surface potential, and ion binding in the crystalline gel phase [21] and interdigitated bilayers [61]. The gel-to-fluid transition of DSPG occurs near 54 °C [2,60–62]. As a consequence, only one set of structural parameters at 60 °C is available from our data analysis (Fig. 3). Compared to DPPG at the same temperature, DSPG has a smaller lipid area and a thicker bilayer.

3.4. Structure of POPG and SOPG

POPG is one of the most biologically relevant and abundant anionic lipids in nature. Though rare in most mammalian cells, it is an important component of pulmonary lung surfactant, where it is believed to play a specialized role in the defense against bacterial and viral infection. In *treponemal* membranes, for example, POPG is reported to: a) interfere with the function of the receptors regulating pathogen associated molecular patterns; b) inhibit the production of proinflammatory cytokine; c) depress abscess formation; and d) modulate immune responses [81]. Other studies have found that POPG inhibits bacterial lipopolysaccharide (LPS) induced production of the proinflammatory mediator, cytokine, by interacting with the LPS binding protein [82], and it suppresses the proinflammatory action of *Mycoplasma pneumoniae* by reducing arachidonic acid release from macrophages [83]. POPG has also been shown to bind the respiratory syncytial virus with high affinity, inhibiting its attachment to epithelial cells [84].

Similarly to PG lipids with saturated hydrocarbon chains, the presence of divalent cations perturbs the phase behavior of POPG [85]. The main gel-to-liquid crystalline transition in POPG bilayers occurs below 0 °C [85–87]. The structural parameters of POPG at four different temperatures, as well as linear fits and estimated uncertainties, are shown in Fig. 4. It is clear from the figure that the replacement of a single bond with a double bond does not significantly attenuate the thermal response (compared to saturated lipids, POPG exhibits a similar temperature dependence for A, D_B, and $2D_C$).

As in the case of DMPG bilayers, we were unable to find lipid area measurements for synthetic POPG bilayers in the literature, although PG synthesized from egg-PC (and presumably rich in palmitoyl-oleoyl chains) has a reported area per lipid of 67.5 $Å^2$ at room temperature [19], a value determined by osmotic swelling [88]. This value for area per lipid is larger than our interpolated value of 64.7 $Å^2$. It has been mentioned previously that lipid areas obtained from MD simulations often do not agree with experimentally determined values [29]. A large variability in POPG lipid areas at 37 °C has been reported from MD simulations, namely: 66.4 $Å^2$ [12]; 65 $Å^2$ [19]; 64.2 $Å^2$ [13]; 49–51 $Å^2$ in association with various cations, and 68.2 $Å^2$ for a POPG/potassium complex [17]; 55–57 $Å^2$ [16]; 56 $Å^2$ [15]; 53 $Å^2$ [89]; and 62.8 $Å^2$ [10]. With the exception of the POPG/potassium complex [17], each of these POPG areas is smaller than our interpolated value of 67.3 $Å^2$.

We also studied SOPG, which has two additional methylene groups in its saturated *sn*-1 chain, compared to POPG. Our volume and scattering data suggest that the main phase transition temperature of SOPG bilayers occurs below 20 °C, consistent with the known SOPC transition temperature of 6 °C [90]. A small peak near 0.1 $Å^{-1}$, present in the X-ray form factors at 20 and 30 °C (Supplementary Figs. S16 and S17), is most likely due to the presence of pauci-lamellar vesicles (PLV). As a result, much larger error uncertainties are assigned to the data points in the vicinity of this peak region in order to diminish any PLV influence. Interestingly, this peak disappeared with increasing temperature, and was also absent in the neutron form factors which determine the bilayer's overall thickness and area per lipid. The structural parameters of SOPG bilayers are shown in Fig. 4. In general, the thermal response of SOPG bilayers is very similar to that of POPG, and slightly less pronounced than bilayers with saturated chain lipids.

3.5. Structure of DOPG

It has previously been shown that interactions between phospholipids and cholesterol depend on the degree of phospholipid chain unsaturation [91,92]. The immiscibility of di-monounsaturated lipids with cholesterol and saturated lipids has served as the prototypical model for phase separation and lateral domain formation [93,94]. To investigate how the degree of chain unsaturation affects the structure of bilayers composed of anionic PG lipids as a function of

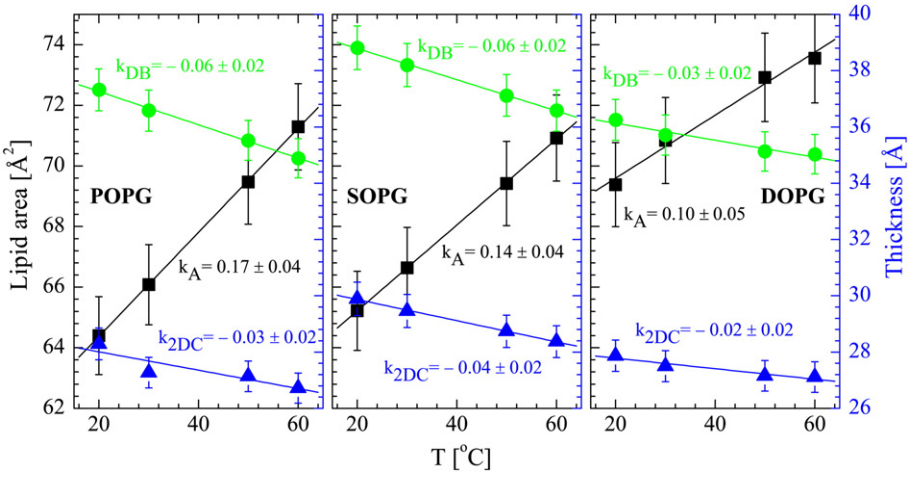

Fig. 4. Temperature dependence of POPG, SOPG, and DOPG lipid areas *A* (black squares), overall bilayer thicknesses D_B (green circles), and hydrocarbon chain thicknesses $2D_C$ (blue triangles). Also shown are the linear least-square fits (solid lines) to the data with slopes denoted by *k* and uncertainties estimated from MC simulations.

temperature, we determined the structure of DOPG bilayers at four temperatures.

The phase behavior of DOPG in response to divalent cations and PC lipids with different chain lengths has been previously reported [95]. The main gel-to-liquid crystalline transition of DOPG bilayers takes place near −18 °C [95], and its structural parameters obtained using SDP model analysis are shown in Fig. 4. Due to the presence of two *cis*-double bonds (i.e., one in each hydrocarbon chain), DOPG possesses the largest area of the lipids in this study. This observation is consistent with the areas of di-monounsaturated PC lipids, with DOPC exhibiting the largest area per lipid [96]. Also, similarly to zwitterionic PC lipid bilayers, the thermal response of DOPG is determined to be about half that of lipids with two saturated chains. In other words, DOPG undergoes much smaller structural changes as a function of temperature, a feature most likely due to an intrinsic disorder associated with having two monounsaturated hydrocarbon chains [38].

4. Discussion

The self-assembly of amphiphilic lipid molecules possessing a polar headgroup and two hydrophobic hydrocarbon chains into a planar bilayer structure is dictated by the delicate, but cooperative balance between lateral attractive and repulsive forces, including hydrophobic, van der Waals, steric, dipole–dipole and electrostatic interactions. Any external or internal factors that alter the balance of these forces will affect the aggregate structure. In the present study we specifically investigated how the structure of model PG lipid bilayers is influenced by temperature, chain composition and headgroup charge.

4.1. The effect of temperature on bilayer structure

In membranes, temperature is a thermodynamic parameter that manifests itself in a number of ways, such as critical thermal fluctuations [97], phase transitions [98], and domain formation [99]. By examining the thermal response of lipid model membranes, a better understanding of the adaptation of cells to their external environment (e.g., through changes in membrane composition, bending rigidity, fluidity, morphology, etc.) can be achieved. The current structural study of PG lipid bilayers at several different temperatures allows us to accurately quantify their temperature dependence at the molecular level. Moreover, a parallel comparison of thermal responses exhibited by lipids with varying chain length and degrees of hydrocarbon chain unsaturation enables us to assess how biological membranes may benefit from lipid diversity. Since biological membranes contain many different lipid species, their overall structure depends, to a great extent, on lipid composition (e.g., the ratio between different lipid components). By incorporating different lipid species in different quantities, membrane structure can be tweaked to create local environments that enable specific membrane functions.

The structural properties of PG bilayers as a function of temperature are illustrated in Figs. 3 and 4. Differences in thermal response are observed for lipids with different degrees of chain unsaturation, with the largest changes taking place in lipids with two fully saturated chains (Fig. 3, Tables 2–4). These findings are consistent with a previous report of PC lipids using the SDP model to simultaneously analyze neutron and X-ray scattering data [38]. A less pronounced temperature dependence in the case of lipids with unsaturated hydrocarbon chains has also been observed by other groups utilizing different experimental and theoretical approaches. For example, using coarse-grained MD simulations, Stevens [100] determined the lipid area thermal expansion coefficient k_A of DOPC to be half that of DMPC. Using the Luzzati method together with a heuristic interpolation, Costigan and coworkers reported a similar trend for DOPC, POPC, and DMPC bilayers [101]. The similarities observed here between neutral (PC) and charged (PG) lipids underscore that the temperature effect on lipid area is, for the most part, manifested through the disordering of the hydrocarbon chains. This implies that already disordered unsaturated hydrocarbon chains are less affected by increasing temperature. In other words, area per lipid for this class of lipids is also less temperature dependent. This attenuation in the effect of temperature on bilayer structural parameters is most likely energetically favorable for organisms which experience periodic temperature variations [102].

A closer examination of the effect of temperature on lipid bilayers reveals that PG and PC lipids with identical hydrocarbon chains exhibit a similar thermal response. For example, the overall bilayer thickness contractivity for DMPC at 30 °C was reported to be 0.0019 K^{-1} [103] and $0.0022 \pm 0.0006\ K^{-1}$ [38], well within the range of our $0.0016 \pm 0.0009\ K^{-1}$ value for DMPG bilayers at 30 °C. Although a different definition for bilayer thickness was applied, Simon and coworkers [104] reported a phosphate–phosphate thickness contractivity of 0.0022 K^{-1} for egg-PC at 23 °C, a value not so dissimilar to the overall thickness we found for POPG bilayers at 20 °C (i.e., $0.0016 \pm 0.0006\ K^{-1}$). Our PG results are also consistent with an earlier NMR study of PC lipids with different chain lengths in which an area expansion coefficient of 0.24–0.29 Å^2 K^{-1} was reported [105]. However, better agreement is observed when comparing previous

SDP-obtained PC data [38] with the present PG data. For example, the area expansion coefficients for DLPC, DMPC, DPPC, POPC, and SOPC are 0.17, 0.19, 0.19, 0.14, and 0.14 $Å^2\,K^{-1}$, respectively [38], and are similar to the values obtained in this study for the corresponding PG lipids (i.e., 0.20, 0.16, 0.25, 0.17, and 0.14 $Å^2\,K^{-1}$). Discrepancies between scattering studies also exist. For example, a previous standalone X-ray study of DOPC reported an area thermal expansion coefficient of 0.21 $Å^2\,K^{-1}$ [106]. This is larger than the upper bound for DOPG bilayers (0.10 ± 0.05 $Å^2\,K^{-1}$), implying possible differences between zwitterionic and anionic lipid bilayers, and/or differences between the different techniques used in the two studies. The need for a more extensive use of experimental data in determining bilayer structural parameters has also been previously emphasized [28].

4.2. The effect of hydrocarbon chains on bilayer structure

Lipid chain diversity (e.g., length and degree of unsaturation) is of paramount importance to biological systems and is closely associated with biological processes, such as the sorting of cholesterol [107] and the hydrophobic matching necessary for the activation/deactivation of certain membrane proteins [108]. In Fig. 5 we plot A, D_B, and $2D_C$ as a function of chain length at various temperatures (i.e., 20, 30, 50, and 60 °C). The area and thickness expansivities with respect to chain length are defined similarly to the temperature expansivity (see Section 2.5), and are determined by linear least-square fits in the case of data sets with two or more data points. The values for these parameters are listed in Tables 2–4. An interesting result is that at constant temperature the areas of lipids with two saturated chains (Fig. 5, left column) decrease as chain length increases, indicating that the attractive van der Waals interactions supersede the repulsive entropic and volume exclusion steric interactions, becoming increasingly important with each additional methylene group. This trend is, however, reversed (20 and 30 °C) or suppressed (50 and 60 °C) by the introduction of a double bond (Fig. 5, middle column). It should be noted that the different trends of chain length dependence in the case of mixed chain lipid areas (i.e., POPG and SOPG) at different temperatures are, for the most part, the result of the heightened sensitivity of POPG's molecular volume to changes in temperature, compared to SOPG (Table 1).

In contrast to lipid area which behaves differently as a function of chain length for different lipids, both D_B and $2D_C$ increase with increasing chain length, as shown in Fig. 5B and C. It is clear from the figure that the slopes are identical for the two thicknesses. Also, because D_B includes the charged PG headgroup, D_B and $2D_C$ having the same slope indicates that the headgroup undergoes negligible conformational change as a function of chain length. This decoupling effect between the lipid's headgroup and its hydrocarbon chains implies the presence of a relatively rigid headgroup, in agreement with our notion that headgroup volume does not change as a function of hydrocarbon chain composition. This is further explored by plotting the volumes of saturated lipids at 60 °C as a function of chain length (not shown). We obtain a linear dependence that intersects the vertical axis at $V = 300.6 \pm 10.0$ $Å^3$, a value consistent with our estimate of $V_{HL} = 291$ $Å^3$ (see Section 2.1).

The effect of chain unsaturation on the various bilayer parameters (i.e., A, D_B, and $2D_C$) has also been reported for PC lipids [38]. It seems that the effect of unsaturation on A is smaller in the case of PG bilayers as the electrostatic interactions between PG headgroups attenuate the disordering effect induced by the presence of an unsaturated bond, whose primary effect is to disrupt chain packing and increase lateral area. To demonstrate the effect that unsaturated bonds have on hydrocarbon chains, we calculate the effective length L of each chain segment as a function of total methylene, methine and methyl groups making-up the hydrocarbon chain [106]. L is defined as $L = Dc/(nCH_2 + r_{12} \times nCH + r)$, where nCH_2 and nCH are the number of methylene and methine groups, and $r_{12} = V(CH)/V(CH_2)$ and $r = V(CH_3)/V(CH_2)$ are volume ratios obtained from the SDP model analysis. Fig. 6 shows that the average L for lipids with two saturated chains increases with chain length. The observed trend indicates that hydrocarbon chains become stiffer with increasing chain length, a notion that is consistent with a larger bending modulus found in bilayers composed of longer-chain lipids [109]. The disordering effect of the unsaturated bond is manifested by a decrease in L (e.g., DSPG vs. SOPG). The addition of another unsaturated hydrocarbon chain (e.g., SOPG vs. DOPG) decreases L further. Interestingly, the changes due to the addition of each double bond are comparable, unlike the case of PC bilayers where the addition of the first double bond increased the area per lipid about twice as much as the addition of a second double bond [33].

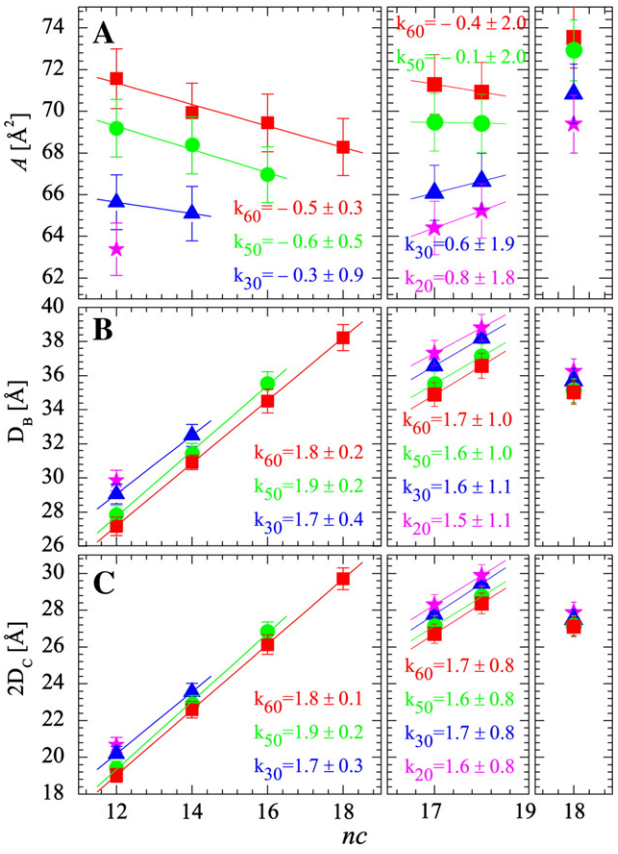

Fig. 5. Chain length nc dependence of lipid areas A (A), overall bilayer thicknesses D_B (B), and hydrocarbon thicknesses $2D_C$ (C) at 60 °C (red squares), 50 °C (green circles), 30 °C (blue triangles), and 20 °C (magenta star), respectively. The left column corresponds to lipids with two saturated chains, the middle column to lipids with a monounsaturated *sn*-2 chain, and the right column corresponds to lipid with two monounsaturated chains. Note that the chain lengths of mixed chain lipids (i.e., POPG and SOPG) are averaged over their hydrocarbon chains (middle column). Linear least-square fits (solid lines) are shown for data sets with two or more data points, with corresponding slopes (k) and estimated uncertainties from MC simulations.

The equilibrated lipid area is governed by a balance of forces resulting from the headgroup and hydrocarbon chains. In the infinitely long chain length regime, where lipid chain–chain van der Waals attractive interactions dominate (i.e., headgroup electrostatic interactions are negligible), the headgroup has a minimum area due to the steric interactions between the interfacial glycerol–carbonyl groups. However, the observed minimal area is still larger than the optimum packing for all-trans chains [105], indicating that the overall lipid area is determined by the headgroup steric limit. Because both PG and PC lipids share the same glycerol–carbonyl ester linkage, the limiting area is expected to be the same. Indeed, by extrapolating to $1/nc = 0$, one observes that lipid areas for PG and PC lipids are similar

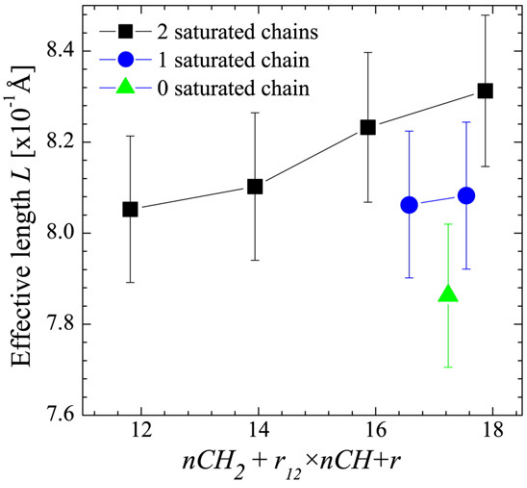

Fig. 6. The effective length L of PG lipid hydrocarbon chains along the bilayer normal at 60 °C as a function of the effective number of carbons. The disordering effect of an unsaturated bond is reflected by the smaller L values with increasing levels of chain unsaturation.

(Fig. 7A). Our limiting areas at $1/nc = 0$ are also in good agreement with those from an earlier report of PC lipids obtained from NMR measurements [105], although a more complicated relation between chain length and lipid area was used. The observed similar limiting areas are consistent with the general consensus that the headgroup is fully solvated, with some water molecules penetrating the headgroup–hydrocarbon chain interface [110]. When a greater lateral attractive pressure [111,112] is exerted, due to the presence of a longer hydrocarbon chain, these interfacial water molecules are expelled (possibly all of them), at which point the carbonyl–glycerol backbone hinders any further lateral contraction, and a limiting area is reached. The aforementioned mechanism is most informative when it comes to explaining the differences between lipids with ether and ester linkages [113,114].

As chain length decreases from infinity, lateral chain packing area increases due to attenuated chain–chain interactions, until it exceeds the headgroup steric area. Beyond that point, the overall area is dictated by chain–chain, headgroup–headgroup and headgroup–chain interactions. Due to the anionic nature of PG lipids, the additional

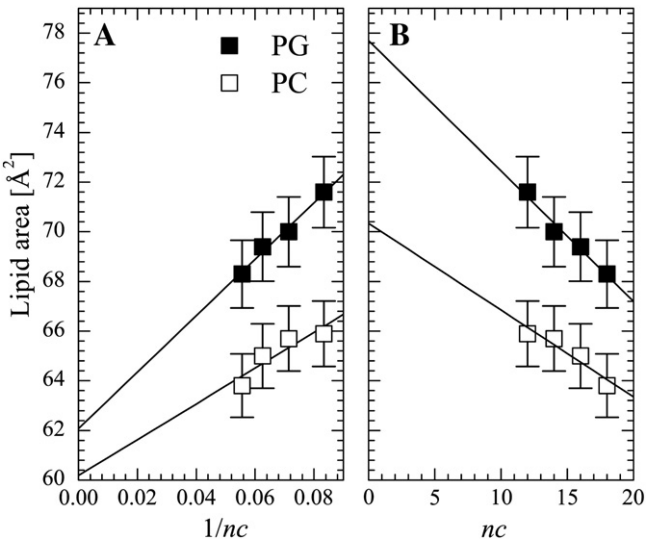

Fig. 7. Lipid areas for saturated PG (present data) and PC [38] lipids at 60 °C as a function of chain length nc. Extrapolating to $1/nc = 0$ (A) gives rise to an area per lipid of 62.0 ± 4.6 Å^2 (PG) and 60.2 ± 4.3 Å^2 (PC), respectively. When $nc = 0$ (B) the area per lipid is 77.7 ± 4.8 Å^2 and 70.3 ± 4.4 Å^2 for PG and PC lipids, respectively.

repulsive electrostatic interactions contribute to the larger areas associated with PG lipids. The area difference between PG and PC lipids is maximal at zero chain length (Fig. 7B) — note that although $nc = 0$ does not correspond to a physical state of the lipid bilayer, this limiting area reflects, however, the headgroup's effect on the lipid's lateral packing behavior.

4.3. The effect of headgroup on bilayer structure

The importance of lipid headgroups is implied by the fact that they reside at the interface separating the bilayer's hydrophobic hydrocarbon interior from bulk water. Importantly, headgroup diversity modulates electrostatic potential in and near the membrane surface, a feature central to a wide range of biological processes [115,116].

Similarly to previous results, the examination of headgroup tilt reveals a difference between PG and PC lipids with unsaturated chains. A crude measure of headgroup tilt can be calculated from the centers of the Gaussians describing the transverse distribution of the two headgroup components (i.e., phosphate and terminal glycerol for PG, and phosphate-CH_2CH_2N and choline methyls for PC) and an estimate of the distance across these headgroups. We find approximately a 10° tilt for both PG and PC lipids with one unsaturated chain. Also, this tilt seems to decrease to a value close to zero (i.e., headgroup is oriented parallel to the plane of the membrane) in PG bilayers made up of fully saturated chains, while it increases in PC bilayers. On the other hand, this spread in headgroup tilt values may point to an inadequacy in the SDP model regarding this parameter. This inadequacy would be consistent with results previously reported [29], where a direct comparison of experimental and simulated results suggested a difference in headgroup tilt angle of 20°, while little difference was seen in the other structural parameters.

Results from the SDP analysis show that the areas of charged PG lipids are larger than their neutral PC counterparts by about 4 Å^2, despite the fact that the PG headgroup volume is smaller (Table 2). For lipids with one or more unsaturated chains, area differences between PG and PC lipids become smaller, i.e., ~2 Å^2. As mentioned, the disordering effect resulting from the introduction of a double bond attenuates the contribution of the charged headgroup to lateral expansion. Consequently, smaller area differences are observed between PG and PC lipids with unsaturated chains.

The double layer Gouy–Chapman theory predicts that the unit free energy of a charged interface submerged in an ionic solution is proportional to its surface charge density. A larger lipid area and a concomitantly smaller surface charge density are thus energetically favorable in the case of PG lipids. Lipid areas play central roles in regulating membrane permeability and stability. The obtained larger areas for charged lipids are consistent with the finding that the introduction of anionic PG lipids results in a reduced membrane rupture pressure, a feature associated with membrane stability [117]. The larger PG areas may also play important roles in regulating protein translocation [118], modulating bacterial membrane permeability [119], and enhancing membrane protein folding [120].

5. Conclusions

We obtained neutron and X-ray scattering data of commonly used, fluid PG bilayers as a function of temperature. The reduced experimental form factors were used to compare directly to simulated data and for model-based analysis. Specifically, we applied the recently developed SDP model for anionic PG lipids [29] to simultaneously analyze these data with input from MD simulations and volume measurements. The notable findings of this analysis can be summarized as follows: a) despite their smaller lipid volumes, PG lipid areas were found to be larger than their corresponding PC counterparts, most likely the result of electrostatic interactions taking place within the headgroup region — a region which is critical for

specific interactions with surface associated molecules [121]; b) the molecular structure of PG lipids as a function of temperature and chain length revealed that they behave similarly to PC lipids; c) the inclusion of unsaturated hydrocarbon chains attenuates temperature induced structural changes; d) through extrapolation, the lipid area of saturated PG lipids at infinite chain length was determined to be similar to that of PC lipids, highlighting the importance of the glycerol–carbonyl backbone in dictating the nature of the interactions taking place at the lipid–water interface.

Acknowledgements

This work acknowledges the support of the office of Biological and Environmental Research at Oak Ridge National Laboratory's (ORNL) Center for Structural Molecular Biology (CSMB) through the utilization of facilities supported by the U.S. Department of Energy, managed by UT-Battelle, LLC under contract no. DE-AC05-00OR2275. Facilities located at the National Institute of Standards and Technology (NIST) are supported in part by the National Science Foundation under agreement no. DMR-0944772. Facilities located at the Cornell High Energy Synchrotron Source (CHESS), are supported by the National Science Foundation and the National Institutes of Health/National Institute of General Medical Sciences under National Science Foundation award DMR-0225180. JK is supported by ORNL's Program Development (PD) and Laboratory Directed Research and Development (LDRD) programs. STN is supported in part by NIH Grant GM 44976, and the Charles E. Kaufman Foundation. STN would like to acknowledge John Nagle for useful discussions.

Appendix A. Supplementary material

Supplementary data to this article can be found online at http://dx.doi.org/10.1016/j.bbamem.2012.05.007.

References

[1] W. Dowhan, Molecular basis for membrane phospholipid diversity: why are there so many lipids, Annu. Rev. Biochem. 66 (1997) 199–232.
[2] Y.P. Zhang, R.N.A.H. Lewis, R.N. McElhaney, Calorimetric and spectroscopic studies of the thermotropic phase behavior of the n-saturated 1,2-diacylphosphatidylglycerols, Biophys. J. 72 (1997) 779–793.
[3] H. Wada, N. Mizusawa, The role of phosphatidylglycerol in photosynthesis, in: H. Wada, N. Murata (Eds.), Lipids in Photosynthesis: Essential and Regulatory Functions, Springer, Dordrecht, The Netherlands, 2009.
[4] F.J. Weber, J.A.M. de Bont, Adaptation mechanisms of microorganisms to the toxic effects of organic solvents on membranes, Biochim. Biophys. Acta Rev. Biomembr. 1286 (1996) 225–245.
[5] M. Zasloff, Antimicrobial peptides of multicellular organisms, Nature 415 (2002) 389–395.
[6] A. Peschel, R.W. Jack, M. Otto, L.V. Collins, P. Staubitz, G. Nicholson, H. Kalbacher, W.F. Nieuwenhuizen, G. Jung, A. Tarkowski, K.P.M. van Kessel, J.A.G. van Strijp, *Staphylococcus aureus* resistance to human defensins and evasion of neutrophil killing via the novel virulence factor MprF is based on modification of membrane lipids with L-lysine, J. Exp. Med. 193 (2001) 1067–1076.
[7] H. Nishi, H. Komatsuzawa, T. Fujiwara, N. McCallum, M. Sugai, Reduced content of lysyl-phosphatidylglycerol in the cytoplasmic membrane affects susceptibility to moenomycin, as well as vancomycin, gentamicin, and antimicrobial peptides, in *Staphylococcus aureus*, Antimicrob. Agents Chemother. 48 (2004) 4800–4807.
[8] C. Sohlenkamp, K.A. Galindo-Lagunas, Z.Q. Guan, P. Vinuesa, S. Robinson, J. Thomas-Oates, C.R.H. Raetz, O. Geiger, The lipid lysyl-phosphatidylglycerol is present in membranes of *Rhizobium tropici* CIAT899 and confers increased resistance to polymyxin B under acidic growth conditions, Mol. Plant Microbe Interact. 20 (2007) 1421–1430.
[9] T. Rog, K. Murzyn, M. Pasenkiewicz-Gierula, Molecular dynamics simulations of charged and neutral lipid bilayers: treatment of electrostatic interactions, Acta Biochim. Pol. 50 (2003) 789–798.
[10] K. Murzyn, T. Rog, M. Pasenkiewicz-Gierula, Phosphatidylethanolamine–phosphatidylglycerol bilayer as a model of the inner bacterial membrane, Biophys. J. 88 (2005) 1091–1103.
[11] W. Zhao, T. Rog, A.A. Gurtovenko, I. Vattulainen, M. Karttunen, Role of phosphatidylglycerols in the stability of bacterial membranes, Biochimie 90 (2008) 930–938.
[12] I.S. Tolokh, V. Vivcharuk, B. Tomberli, C.G. Gray, Binding free energy and counterion release for adsorption of the antimicrobial peptide lactoferricin B on a POPG membrane, Phys. Rev. E 80 (2009) 031911.
[13] C.I. von Deuster, V. Knecht, Competing interactions for antimicrobial selectivity based on charge complementarity, Biochim. Biophys. Acta Biomembr. 1808 (2011) 2867–2876.
[14] A.A. Polyansky, R. Ramaswamy, P.E. Volynsky, I.F. Sbalzarini, S.J. Marrink, R.G. Efremov, Antimicrobial peptides induce growth of phosphatidylglycerol domains in a model bacterial membrane, J. Phys. Chem. Lett. 1 (2010) 3108–3111.
[15] D.E. Elmore, Molecular dynamics simulation of a phosphatidylglycerol membrane, FEBS Lett. 580 (2006) 144–148.
[16] A. Dickey, R. Faller, Examining the contributions of lipid shape and headgroup charge on bilayer behavior, Biophys. J. 95 (2008) 2636–2646.
[17] H.Y. Yang, Y.C. Xu, Z.B. Gao, Y.Y. Mao, Y. Du, H.L. Jiang, Effects of Na(+), K(+), and Ca(2+) on the structures of anionic lipid bilayers and biological implication, J. Phys. Chem. B 114 (2010) 16978–16988.
[18] M. Manna, C. Mukhopadhyay, Molecular dynamics simulations of the interactions of kinin peptides with an anionic POPG bilayer, Langmuir 27 (2011) 3713–3722.
[19] J. Henin, W. Shinoda, M.L. Klein, Models for phosphatidylglycerol lipids put to a structural test, J. Phys. Chem. B 113 (2009) 6958–6963.
[20] T. Broemstrup, N. Reuter, Molecular dynamics simulations of mixed acidic/zwitterionic phospholipid bilayers, Biophys. J. 99 (2010) 825–833.
[21] J. Marra, Direct measurement of the interaction between phosphatidylglycerol bilayers in aqueous electrolyte solutions, Biophys. J. 50 (1986) 815–825.
[22] K. Tajima, Y. Imai, T. Horiuchi, M. Koshinuma, A. Nakamura, ESR study on DMPC and DMPG bilayers in the (L(alpha)+H_2O) phase, Langmuir 12 (1996) 6651–6658.
[23] J.N. Sachs, H.I. Petrache, T.B. Woolf, Interpretation of small angle X-ray measurements guided by molecular dynamics simulations of lipid bilayers, Chem. Phys. Lipids 126 (2003) 211–223.
[24] J.B. Klauda, B.R. Brooks, R.W. Pastor, Dynamical motions of lipids and a finite size effect in simulations of bilayers, J. Chem. Phys. 125 (2006) 144710.
[25] J.B. Klauda, R.M. Venable, J.A. Freites, J.W. O'Connor, D.J. Tobias, C. Mondragon-Ramirez, I. Vorobyov, A.D. MacKerell, R.W. Pastor, Update of the CHARMM all-atom additive force field for lipids: validation on six lipid types, J. Phys. Chem. B 114 (2010) 7830–7843.
[26] C. Anezo, A.H. de Vries, H.D. Holtje, D.P. Tieleman, S.J. Marrink, Methodological issues in lipid bilayer simulations, J. Phys. Chem. B 107 (2003) 9424–9433.
[27] J.F. Nagle, S. Tristram-Nagle, Structure of lipid bilayers, Biochim. Biophys. Acta Rev. Biomembr. 1469 (2000) 159–195.
[28] N. Kučerka, J.F. Nagle, J.N. Sachs, S.E. Feller, J. Pencer, A. Jackson, J. Katsaras, Lipid bilayer structure determined by the simultaneous analysis of neutron and X-ray scattering data, Biophys. J. 95 (2008) 2356–2367.
[29] N. Kučerka, B.W. Holland, C.G. Gray, B. Tomberli, J. Katsaras, Scattering density profile model of POPG bilayers as determined by molecular dynamics simulations and small-angle neutron and X-ray scattering experiments, J. Phys. Chem. B 116 (2012) 232–239.
[30] N. Kučerka, J. Pencer, J.N. Sachs, J.F. Nagle, J. Katsaras, Curvature effect on the structure of phospholipid bilayers, Langmuir 23 (2007) 1292–1299.
[31] J.F. Nagle, D.A. Wilkinson, Lecithin bilayers. Density measurements and molecular interactions, Biophys. J. 23 (1978) 159–175.
[32] M.C. Wiener, S. Tristram-Nagle, D.A. Wilkinson, L.E. Campbell, J.F. Nagle, Specific volumes of lipids in fully hydrated bilayer dispersions, Biochim. Biophys. Acta Biomembr. 938 (1988) 135–142.
[33] N. Kučerka, S. Tristram-Nagle, J.F. Nagle, Structure of fully hydrated fluid phase lipid bilayers with monounsaturated chains, J. Membr. Biol. 208 (2005) 193–202.
[34] N. Kučerka, Y.F. Liu, N.J. Chu, H.I. Petrache, S.T. Tristram-Nagle, J.F. Nagle, Structure of fully hydrated fluid phase DMPC and DLPC lipid bilayers using X-ray scattering from oriented multilamellar arrays and from unilamellar vesicles, Biophys. J. 88 (2005) 2626–2637.
[35] S. Tristram-Nagle, H.I. Petrache, J.F. Nagle, Structure and interactions of fully hydrated dioleoylphosphatidylcholine bilayers, Biophys. J. 75 (1998) 917–925.
[36] A.I. Greenwood, S. Tristram-Nagle, J.F. Nagle, Partial molecular volumes of lipids and cholesterol, Chem. Phys. Lipids 143 (2006) 1–10.
[37] S. Tristram-Nagle, Y.F. Liu, J. Legleiter, J.F. Nagle, Structure of gel phase DMPC determined by X-ray diffraction, Biophys. J. 83 (2002) 3324–3335.
[38] N. Kučerka, M.P. Nieh, J. Katsaras, Fluid phase lipid areas and bilayer thicknesses of commonly used phosphatidylcholines as a function of temperature, Biochim. Biophys. Acta Biomembr. 1808 (2011) 2761–2771.
[39] N. Kučerka, J. Katsaras, J.F. Nagle, Comparing membrane simulations to scattering experiments: introducing the SIMtoEXP software, J. Membr. Biol. 235 (2010) 43–50.
[40] C.J. Glinka, J.G. Barker, B. Hammouda, S. Krueger, J.J. Moyer, W.J. Orts, The 30 m small-angle neutron scattering instruments at the National Institute of Standards and Technology, J. Appl. Crystallogr. 31 (1998) 430–445.
[41] G.W. Lynn, W. Heller, V. Urban, G.D. Wignall, K. Weiss, D.A.A. Myles, Bio-SANS — a dedicated facility for neutron structural biology at oak ridge national laboratory, Physica B 385–86 (2006) 880–882.
[42] S.R. Kline, Reduction and analysis of SANS and USANS data using IGOR Pro, J. Appl. Crystallogr. 39 (2006) 895–900.
[43] M.C. Wiener, S.H. White, Fluid bilayer structure determination by the combined use of X-ray and neutron-diffraction. 1. Fluid bilayer models and the limits of resolution, Biophys. J. 59 (1991) 162–173.
[44] V. Luzzati, F. Husson, The structure of the liquid-crystalline phases of lipid–water systems, J. Cell Biol. 12 (1962) 207–219.
[45] W.H. Press, S.A. Teukolsky, W.T. Vetterling, B.P. Flannery, Numerical recipes, The Art of Scientific Computing, 3rd edition, Cambridge University Press, 2007.
[46] A.J. Verkleij, B. de Kruyff, P.H.J.Th. Ververgaert, J.F. Tocanne, L.L.M. van Deenen, The influence of pH, Ca^{2+} and protein on the thermotropic behaviour of the

negatively charged phospholipid, phosphatidylglycerol, Biochim. Biophys. Acta Biomembr. 339 (1974) 432–437.
[47] J.F. Tocanne, P.H.J.Th. Ververgaert, A.J. Verkleij, L.L.M. van Deenen, A monolayer and freeze-etching study of charged phospholipids. I. Effects of ions and pH on the ionic properties of phosphatidylglycerol and lysylphosphatidylglycerol, Chem. Phys. Lipids 12 (1974) 201–219.
[48] M.M. Sacre, J.F. Tocanne, Importance of glycerol and fatty acid residues on the ionic properties of phosphatidylglycerols at the air–water interface, Chem. Phys. Lipids 18 (1977) 334–354.
[49] M.M. Sacre, W. Hoffmann, M. Turner, J.F. Tocanne, D. Chapman, Differential scanning calorimetric studies of some phosphatidyl glycerol lipid–water systems, Chem. Phys. Lipids 25 (1979) 69–83.
[50] F. Lakhdar-Ghazal, J.L. Tichadou, J.F. Tocanne, Effect of pH and monovalent cations on the ionization state of phosphatidylglycerol in monolayers — an experimental (surface-potential) and theoretical (Gouy–Chapman) approach, Eur. J. Biochem. 134 (1983) 531–537.
[51] T. Thuren, P. Vainio, J.A. Virtanen, P. Somerharju, K. Blomqvist, P.K.J. Kinnunen, Evidence for the control of the action of phospholipases A by the physical state of the substrate, Biochemistry 23 (1984) 5129–5134.
[52] J.F. Nagle, Theory of the main lipid bilayer phase transition, Annu. Rev. Phys. Chem. 31 (1980) 157–195.
[53] F.M. Marassi, P.M. Macdonald, Response of the headgroup of phosphatidylglycerol to membrane surface charge as studied by deuterium and phosphorus-31 nuclear magnetic resonance, Biochemistry 30 (1991) 10558–10566.
[54] R.M. Epand, B. Gabel, R.F. Epand, A. Sen, S.W. Hui, A. Muga, W.K. Surewicz, Formation of a new stable phase of phosphatidylglycerols, Biophys. J. 63 (1992) 327–332.
[55] K.A. Riske, M.J. Politi, W.F. Reed, M.T. Lamy-Freund, Temperature and ionic strength dependent light scattering of DMPG dispersions, Chem. Phys. Lipids 89 (1997) 31–44.
[56] M.T. Lamy-Freund, K.A. Riske, The peculiar thermo-structural behavior of the anionic lipid DMPG, Chem. Phys. Lipids 122 (2003) 19–32.
[57] F. Spinozzi, L. Paccamiccio, P. Mariani, L.Q. Amaral, Melting regime of the anionic phospholipid DMPG: new lamellar phase and porous bilayer model, Langmuir 26 (2010) 6484–6493.
[58] J.M. Alakoskela, M.J. Parry, P.K.J. Kinnunen, The intermediate state of DMPG is stabilized by enhanced positive spontaneous curvature, Langmuir 26 (2010) 4892–4900.
[59] K.K. Eklund, J.A. Virtanen, K. Vuori, J. Patrikainen, P.K.J. Kinnunen, Role of the polar head group stereoconfiguration in the cation-induced aggregation of dimyristoylphosphatidylglycerol vesicles, Biochemistry 26 (1987) 7542–7545.
[60] J.M. Boggs, G. Rangaraj, Phase transitions and fatty acid spin label behavior in interdigitated lipid phases induced by glycerol and polymyxin, Biochim. Biophys. Acta 816 (1985) 221–233.
[61] G. Pabst, S. Danner, S. Karmakar, G. Deutsch, V.A. Raghunathan, On the propensity of phosphatidylglycerols to form interdigitated phases, Biophys. J. 93 (2007) 513–525.
[62] T.P.W. McMullen, R.N.A.H. Lewis, R.N. McElhaney, Calorimetric and spectroscopic studies of the effects of cholesterol on the thermotropic phase behavior and organization of a homologous series of linear saturated phosphatidylglycerol bilayer membranes, Biochim. Biophys. Acta Biomembr. 1788 (2009) 345–357.
[63] R.F. Epand, L. Maloy, A. Ramamoorthy, R.M. Epand, Amphipathic helical cationic antimicrobial peptides promote rapid formation of crystalline states in the presence of phosphatidylglycerol: lipid clustering in anionic membranes, Biophys. J. 98 (2010) 2564–2573.
[64] A. Watts, K. Harlos, W. Maschke, D. Marsh, Control of the structure and fluidity of phosphatidylglycerol bilayers by pH titration, Biochim. Biophys. Acta Biomembr. 510 (1978) 63–74.
[65] A. Watts, K. Harlos, D. Marsh, Charge-induced tilt in ordered-phase phosphatidylglycerol bilayers — evidence from X-ray diffraction, Biochim. Biophys. Acta Biomembr. 645 (1981) 91–96.
[66] G. Degovics, A. Latal, K. Lohner, X-ray studies on aqueous dispersions of dipalmitoyl phosphatidylglycerol in the presence of salt, J. Appl. Crystallogr. 33 (2000) 544–547.
[67] D. Papahadjopoulos, W.J. Vail, W.A. Pangborn, G. Poste, Studies on membrane fusion. II. Induction of fusion in pure phospholipid membranes by calcium ions and other divalent metals, Biochim. Biophys. Acta Biomembr. 448 (1976) 265–283.
[68] D.A. Wilkinson, T.J. Mcintosh, A subtransition in a phospholipid with a net charge, dipalmitoylphosphatidylglycerol, Biochemistry 25 (1986) 295–298.
[69] A.E. Blaurock, T.J. McIntosh, Structure of the crystalline bilayer in the subgel phase of dipalmitoylphosphatidylglycerol, Biochemistry 25 (1986) 299–305.
[70] B. Tenchov, R. Koynova, G. Rapp, New ordered metastable phases between the gel and subgel phases in hydrated phospholipids, Biophys. J. 80 (2001) 1873–1890.
[71] J. Katsaras, V.A. Raghunathan, E.J. Dufourc, J. Dufourcq, Evidence for a two-dimensional molecular lattice in subgel phase DPPC bilayers, Biochemistry 34 (1995) 4684–4688.
[72] V.A. Raghunathan, J. Katsaras, Structure of the L(C′) phase in a hydrated lipid multilamellar system, Phys. Rev. Lett. 74 (1995) 4456–4459.
[73] K.K. Eklund, P.K.J. Kinnunen, Effects of polyamines on the thermotropic behavior of dipalmitoylphosphatidylglycerol, Chem. Phys. Lipids 39 (1986) 109–117.
[74] K.K. Eklund, I.S. Salonen, P.K.J. Kinnunen, Monovalent cation dependent phase behavior of dipalmitoylphosphatidylglycerol, Chem. Phys. Lipids 50 (1989) 71–78.
[75] D. Zubiri, A. Domecq, D.L. Bernik, Phase behavior of phosphatidylglycerol bilayers as a function of buffer composition: fluorescence studies using Laurdan probe, Colloids Surf. B Biointerfaces 13 (1999) 13–28.
[76] D.A. Wilkinson, D.A. Tirrell, A.B. Turek, T.J. McIntosh, Tris buffer causes acyl chain interdigitation in phosphatidylglycerol, Biochim. Biophys. Acta Biomembr. 905 (1987) 447–453.
[77] F. Prossnigg, A. Hickel, G. Pabst, K. Lohner, Packing behaviour of two predominant anionic phospholipids of bacterial cytoplasmic membranes, Biophys. Chem. 150 (2010) 129–135.
[78] P. Wydro, K. Witkowska, The interactions between phosphatidylglycerol and phosphatidylethanolamines in model bacterial membranes: the effect of the acyl chain length and saturation, Colloids Surf. B Biointerfaces 72 (2009) 32–39.
[79] Y.N. Kaznessis, S. Kim, R.G. Larson, Simulations of zwitterionic and anionic phospholipid monolayers, Biophys. J. 82 (2002) 1731–1742.
[80] M. Pickholz, O.N. Oliveira Jr., M.S. Skaf, Interactions of chlorpromazine with phospholipid monolayers: effects of the ionization state of the drug, Biophys. Chem. 125 (2007) 425–434.
[81] M. Hashimoto, Y. Asai, T. Ogawa, Treponemal phospholipids inhibit innate immune responses induced by pathogen-associated molecular patterns, J. Biol. Chem. 278 (2003) 44205–44213.
[82] M. Mueller, K. Brandenburg, R. Dedrick, A.B. Schromm, U. Seydel, Phospholipids inhibit lipopolysaccharide (LPS)-induced cell activation: a role for LPS-binding protein, J. Immunol. 174 (2005) 1091–1096.
[83] P. Kandasamy, S. Zarini, E.D. Chan, C.C. Leslie, R.C. Murphy, D.R. Voelker, Pulmonary surfactant phosphatidylglycerol inhibits *Mycoplasma pneumoniae*-stimulated eicosanoid production from human and mouse macrophages, J. Biol. Chem. 286 (2011) 7841–7853.
[84] M. Numata, H.W. Chu, A. Dakhama, D.R. Voelker, Pulmonary surfactant phosphatidylglycerol inhibits respiratory syncytial virus-induced inflammation and infection, Proc. Natl. Acad. Sci. U. S. A. 107 (2010) 320–325.
[85] F. Borle, J. Seelig, Ca^{2+} binding to phosphatidylglycerol bilayers as studied by differential scanning calorimetry and ^{2}H- and ^{31}P-nuclear magnetic resonance, Chem. Phys. Lipids 36 (1985) 263–283.
[86] T. Wiedmann, A. Salmon, V. Wong, Phase behavior of mixtures of DPPC and POPG, Biochim. Biophys. Acta Lipids Lipid Metab. 1167 (1993) 114–120.
[87] B. Pozo Navas, K. Lohner, G. Deutsch, E. Sevcsik, K.A. Riske, R. Dimova, P. Garidel, G. Pabst, Composition dependence of vesicle morphology and mixing properties in a bacterial model membrane system, Biochim. Biophys. Acta Biomembr. 1716 (2005) 40–48.
[88] A.C. Cowley, N.L. Fuller, R.P. Rand, V.A. Parsegian, Measurement of repulsive forces between charged phospholipid bilayers, Biochemistry 17 (1978) 3163–3168.
[89] W. Zhao, T. Rog, A.A. Gurtovenko, I. Vattulainen, M. Karttunen, Atomic-scale structure and electrostatics of anionic palmitoyloleoylphosphatidylglycerol lipid bilayers with Na^{+} counterions, Biophys. J. 92 (2007) 1114–1124.
[90] C. Vilcheze, T.P.W. McMullen, R.N. McElhaney, R. Bittman, The effect of side-chain analogues of cholesterol on the thermotropic phase behavior of 1-stearoyl-2-oleoylphosphatidylcholine bilayers: a differential scanning calorimetric study, Biochim. Biophys. Acta Biomembr. 1279 (1996) 235–242.
[91] J.J. Pan, T.T. Mills, S. Tristram-Nagle, J.F. Nagle, Cholesterol perturbs lipid bilayers nonuniversally, Phys. Rev. Lett. 100 (2008) 198103.
[92] J.J. Pan, S. Tristram-Nagle, J.F. Nagle, Effect of cholesterol on structural and mechanical properties of membranes depends on lipid chain saturation, Phys. Rev. E 80 (2009) 021931.
[93] G.W. Feigenson, Phase diagrams and lipid domains in multicomponent lipid bilayer mixtures, Biochim. Biophys. Acta Biomembr. 1788 (2009) 47–52.
[94] D. Lingwood, K. Simons, Lipid rafts as a membrane-organizing principle, Science 327 (2010) 46–50.
[95] E.J. Findlay, P.G. Barton, Phase behavior of synthetic phosphatidylglycerols and binary mixtures with phosphatidylcholines in presence and absence of calcium ions, Biochemistry 17 (1978) 2400–2405.
[96] N. Kučerka, J. Gallová, D. Uhríková, P. Balgavý, M. Bulacu, S.J. Marrink, J. Katsaras, Areas of monounsaturated diacylphosphatidylcholines, Biophys. J. 97 (2009) 1926–1932.
[97] S.L. Veatch, O. Soubias, S.L. Keller, K. Gawrisch, Critical fluctuations in domain-forming lipid mixtures, Proc. Natl. Acad. Sci. U. S. A. 104 (2007) 17650–17655.
[98] S. Mabrey, J.M. Sturtevant, Investigation of phase transitions of lipids and lipid mixtures by high sensitivity differential scanning calorimetry, Proc. Natl. Acad. Sci. U. S. A. 73 (1976) 3862–3866.
[99] T. Baumgart, S.T. Hess, W.W. Webb, Imaging coexisting fluid domains in biomembrane models coupling curvature and line tension, Nature 425 (2003) 821–824.
[100] M.J. Stevens, Coarse-grained simulations of lipid bilayers, J. Chem. Phys. 121 (2004) 11942–11948.
[101] S.C. Costigan, P.J. Booth, R.H. Templer, Estimations of lipid bilayer geometry in fluid lamellar phases, Biochim. Biophys. Acta Biomembr. 1468 (2000) 41–54.
[102] J.R. Hazel, E.E. Williams, The role of alterations in membrane lipid composition in enabling physiological adaptation of organisms to their physical environment, Prog. Lipid Res. 29 (1990) 167–227.
[103] V.I. Gordeliy, V.G. Cherezov, J. Teixeira, Evidence of entropic contribution to "hydration" forces between membranes. 2. Temperature dependence of the "hydration" force: a small angle neutron scattering study, J. Mol. Struct. 383 (1996) 117–124.
[104] S.A. Simon, S. Advani, T.J. McIntosh, Temperature dependence of the repulsive pressure between phosphatidylcholine bilayers, Biophys. J. 69 (1995) 1473–1483.
[105] H.I. Petrache, S.W. Dodd, M.F. Brown, Area per lipid and acyl length distributions in fluid phosphatidylcholines determined by (2)H NMR spectroscopy, Biophys. J. 79 (2000) 3172–3192.
[106] J.J. Pan, S. Tristram-Nagle, N. Kučerka, J.F. Nagle, Temperature dependence of structure, bending rigidity, and bilayer interactions of dioleoylphosphatidylcholine bilayers, Biophys. J. 94 (2008) 117–124.
[107] C.J. Fielding, P.E. Fielding, Intracellular cholesterol transport, J. Lipid Res. 38 (1997) 1503–1521.
[108] A.G. Lee, How lipids affect the activities of integral membrane proteins, Biochim. Biophys. Acta Biomembr. 1666 (2004) 62–87.

[109] W. Rawicz, K.C. Olbrich, T. McIntosh, D. Needham, E. Evans, Effect of chain length and unsaturation on elasticity of lipid bilayers, Biophys. J. 79 (2000) 328–339.
[110] D.P. Tieleman, S.J. Marrink, H.J.C. Berendsen, A computer perspective of membranes: molecular dynamics studies of lipid bilayer systems, Biochim. Biophys. Acta Rev. Biomembr. 1331 (1997) 235–270.
[111] D. Marsh, Lateral pressure in membranes, Biochim. Biophys. Acta Rev. Biomembr. 1286 (1996) 183–223.
[112] R.S. Cantor, Lipid composition and the lateral pressure profile in bilayers, Biophys. J. 76 (1999) 2625–2639.
[113] G. Brezesinski, A. Dietrich, B. Struth, C. Bohm, W.G. Bouwman, K. Kjaer, H. Mohwald, Influence of ether linkages on the structure of double-chain phospholipid monolayers, Chem. Phys. Lipids 76 (1995) 145–157.
[114] S.D. Guler, D.D. Ghosh, J.J. Pan, J.C. Mathai, M.L. Zeidel, J.F. Nagle, S. Tristram-Nagle, Effects of ether vs. ester linkage on lipid bilayer structure and water permeability, Chem. Phys. Lipids 160 (2009) 33–44.
[115] S. McLaughlin, The electrostatic properties of membranes, Annu. Rev. Biophys. Biophys. Chem. 18 (1989) 113–136.
[116] G. Cevc, Membrane electrostatics, Biochim. Biophys. Acta 1031 (1990) 311–382.
[117] S.D. Shoemaker, T.K. Vanderlick, Intramembrane electrostatic interactions destabilize lipid vesicles, Biophys. J. 83 (2002) 2007–2014.
[118] T. de Vrije, R.L. de Swart, W. Dowhan, J. Tommassen, B. de Kruijff, Phosphatidylglycerol is involved in protein translocation across *Escherichia coli* inner membranes, Nature 334 (1988) 173–175.
[119] H. Nikaido, M. Vaara, Molecular basis of bacterial outer membrane permeability, Microbiol. Rev. 49 (1985) 1–32.
[120] A.M. Seddon, M. Lorch, O. Ces, R.H. Templer, F. Macrae, P.J. Booth, Phosphatidylglycerol lipids enhance folding of an alpha helical membrane protein, J. Mol. Biol. 380 (2008) 548–556.
[121] M. Langner, K. Kubica, The electrostatics of lipid surfaces, Chem. Phys. Lipids 101 (1999) 3–35.